Environmental Toxicology and Pharmacology 74 (2020) 103303

Contents lists available at ScienceDirect

Environmental Toxicology and Pharmacology

journal homepage: www.elsevier.com/locate/etap

Pulmonary toxicity of Fe_2O_3, $ZnFe_2O_4$, $NiFe_2O_4$ and $NiZnFe_4O_8$ nanomaterials: Inflammation and DNA strand breaks

Niels Hadrup[a,*], Anne T. Saber[a], Zdenka O. Kyjovska[a], Nicklas R. Jacobsen[a], Minnamari Vippola[b], Essi Sarlin[b], Yaobo Ding[c,d], Otmar Schmid[c,d], Håkan Wallin[e], Keld A. Jensen[a,*], Ulla Vogel[a,f,*]

[a] National Research Centre for the Working Environment (NFA), 105 Lersø Parkallé, Copenhagen Ø, Denmark
[b] Materials Science and Environmental Engineering, Tampere University, P.O.Box 589, 33014 Tampere University, Finland
[c] Comprehensive Pneumology Center, Member of the German Center for Lung Research, Max-Lebsche-Platz 31, 81377 Munich, Germany
[d] Institute of Lung Biology and Disease, Helmholtz Zentrum München - German Research Center for Environmental Health, Ingolstädter Landstraße 1, 85764, Neuherberg, Germany
[e] National Institute of Occupational Health, Oslo, Norway
[f] Department of Health Technology, Danish Technical University (DTU), DK-2800 Kgs. Lyngby, Denmark

ARTICLE INFO

Keywords:
Nanomaterial
Iron
Nickel
Zinc
Pulmonary
Metal oxides

ABSTRACT

Exposure to metal oxide nanomaterials potentially occurs at the workplace. We investigated the toxicity of two Fe-oxides: Fe_2O_3 nanoparticles and nanorods; and three MFe_2O_4 spinels: $NiZnFe_4O_8$, $ZnFe_2O_4$, and $NiFe_2O_4$ nanoparticles. Mice were dosed 14, 43 or 128 μg by intratracheal instillation. Recovery periods were 1, 3, or 28 days. Inflammation – neutrophil influx into bronchoalveolar lavage (BAL) fluid – occurred for Fe_2O_3 rods (1 day), $ZnFe_2O_4$ (1, 3 days), $NiFe_2O_4$ (1, 3, 28 days), Fe_2O_3 (28 days) and $NiZnFe_4O_8$ (28 days). Conversion of mass-dose into specific surface-area-dose showed that inflammation correlated with deposited surface area and consequently, all these nanomaterials belong to the so-called low-solubility, low-toxicity class. Increased levels of DNA strand breaks were observed for both Fe_2O_3 particles and rods, in BAL cells three days post-exposure. To our knowledge, this is, besides magnetite (Fe_3O_4), the first study of the pulmonary toxicity of MFe_2O_4 spinel nanomaterials.

1. Introduction

Fe_2O_3, and M-Fe_2O_4 spinel nanomaterials (M = e.g. Ni_x,Zn_{1-x}), are relatively low cost-materials and have several technically interesting physicochemical properties, which make them widely used in different industrial productions. The Fe_2O_3 polymorphs hematite (α-Fe_2O_3) and maghemite (γ-Fe_2O_3) and MFe_2O_4 spinels generally have photocatalytic and photoelectron-catalytic properties (AlSalka et al., 2019). Maghemite and MFe_2O_4 spinels also show paramagnetic to superparamagnetic ($NiFe_2O_4$ and $ZnFe_2O_4$) behaviour (Phumying et al., 2013). Consequently applications of MFe_2O_4 spinels include magnetic resonance imaging enhancement (Bárcena et al., 2008), magnetic recording media (Kubo et al., 1982), gas sensing (Gopal Reddy et al., 2000), electrochemical sensing (Hosni et al., 2018), photo-catalysis (Hosni et al., 2018), as well as in environmental remediation and biomedical applications (Ito et al., 2005; Latorre and Rinaldi, 2009; Prasad et al., 2017). Fe_2O_3 and MFe_2O_4 are also strong colorants with Fe_2O_3 being listed as one of the most used nanomaterials used in Europe (100,000–1,000,000 metric tonnes per year) with uses in coating products, fillers, putties, plasters, modelling clay, non-metal-surface treatment products and metal surface treatment products (ECHA, 2019).

Due to the wide-spread use and relative high production volumes of Fe_2O_3 and MFe_2O_3 polymorphs, there is high risk of human inhalation exposure (Ding et al., 2017; Ham et al., 2015; Koponen et al., 2015; Martin et al., 2015; Xing et al., 2015). Even-though Fe_2O_3 and iron spinels are considered low-soluble low toxicity materials, their catalytic properties and presence of Ni and Zn, and Fe trigger a need for elaborate knowledge of their toxicity. In addition, Fe-oxides and -spinels may

Abbreviations: BAL, bronchoalveolar lavage fluid; Bw, body weight

* Corresponding authors at: National Research Centre for the Working Environment, Lersø Parkallé 105, DK-2100, Copenhagen Ø, Denmark.
E-mail addresses: nih@nfa.dk (N. Hadrup), ats@nfa.dk (A.T. Saber), zokyjovska@gmail.com (Z.O. Kyjovska), nrj@nfa.dk (N.R. Jacobsen), minnamari.vippola@tuni.fi (M. Vippola), essi.sarlin@tuni.fi (E. Sarlin), dyb450303@gmail.com (Y. Ding), otmar.schmid@helmholtz-muenchen.de (O. Schmid), Hakan.Wallin@stami.no (H. Wallin), kaj@nfa.dk (K.A. Jensen), ubv@nfa.dk (U. Vogel).

https://doi.org/10.1016/j.etap.2019.103303
Received 29 August 2019; Received in revised form 19 November 2019; Accepted 20 November 2019
Available online 21 November 2019

occur in different shapes such as fibres. Low-solubility high-aspect ratio nanomaterials have raised concern due to their potential asbestos-like properties (Poland et al., 2008). The pulmonary toxicity of iron oxide particles (Fe_2O_3) has been extensively studied. In these inhalation studies no-observed-adverse-effect concentrations were between 0.1 and 32 mg/m^3 (Pauluhn, 2012, 2009; Pauluhn and Wiemann, 2011; Srinivas et al., 2012; Lijuan et al., 2010; Zhou et al., 2003); in intratracheal instillation studies no-observed-adverse-effect levels of Fe_2O_3 were 0.8 and 2 mg/kg bw by (Pirela et al., 2013; Zhu et al., 2008). In contrast, the toxicological knowledge on MFe_2O_4 nanomaterials is sparse. Toxicity *in vitro* has been reported (Al-Qubaisi et al., 2013; Aziz et al., 2018; Tomitaka et al., 2009); but apart from that, current hazard assessments of such MFe_2O_4 polymorphs have to be based on the assessment of pulmonary toxicity of each element separately. Fe, Ni and Zn. Ni compounds are classified as carcinogenic to humans by IARC (IARC, 2012); and their pulmonary toxicity has been reported in several investigations (Dunnick et al., 1995; Horie et al., 1985; Johansson et al., 1992; NTP, 1996; Oller et al., 2008). Likewise, the pulmonary toxicity of ZnO particles has been addressed (Adamcakova-Dodd et al., 2015; Chen et al., 2015; Chuang et al., 2014; Conner et al., 1988; Hadrup et al., 2019a, 2019b; Ho et al., 2011; Jacobsen et al., 2015; Larsen et al., 2016)

To address the knowledge gap on the hazard of MFe_2O_4 nanomaterials and role of their different toxic elements and thereby strengthen the scientific basis for potential read-across, we compared the pulmonary toxicity of: αFe_2O_3 particles (20 − 60 nm in diameter); αFe_2O_3 rods (outer diameter: 40 − 150 nm, length 250 − 600 nm); $ZnFe_2O_4$ particles (15 − 30 nm); $NiFe_2O_4$ particles (20 − 30 nm); $NiZnFe_4O_8$ particles (10 − 30 nm); and, included carbon black Printex 90 particles (CB) (14 nm) as a positive control. These materials were administered to mice by a single intratracheal instillation; after recovery periods of 1, 3, or 28 days, pulmonary inflammation and levels of DNA strand breaks were assessed.

2. Materials and methods

2.1. Materials

The nanomaterials were obtained from NanoAmor (Houston, TX, USA) and were 1) αFe_2O_3 particle, diameter 20 − 60 nm (Fe_2O_3), 2) αFe_2O_3 rod, diameter: 40 − 150 nm, length: 250 − 600 nm (Fe_2O_3 rod), 3) $Ni_{0.5}Zn_{0.5}Fe_2O_4$, diameter: 10 − 30 nm in diameter ($NiZnFe_4O_8$); 4) $ZnFe_2O_4$, diameter: 15 − 30 nm; 5) $NiFe_2O_4$, diameter: 20 − 30 nm ($NiFe_2O_4$) (Table 1). Carbon black Printex 90 particles (CB) served as a reference particle enabling the benchmarking to previous studies (Bourdon et al., 2012b; Halappanavar et al., 2015; Jacobsen et al., 2011, 2007; Moller et al., 2015; Poulsen et al., 2017, 2016; Saber et al., 2012b, 2016, 2012a, 2012c; Vesterdal et al., 2010). Printex-90 carbon black (CB) nanoparticles were a gift from Evonik Degussa (Essen, Germany). The diameter was 14 nm and the specific surface area was 295–338 m^2/g (Jacobsen et al., 2008b; Saber et al., 2005). It was composed of 99% C, 0.8% N, and 0.01% H, and the total content of polycyclic aromatic hydrocarbons was 0.07 mg/g (Jacobsen et al., 2007).

2.2. Dispersion procedures

Nanomaterials were dispersed following the so-called ENPRA dispersion protocol using 0.2 μm filtered, γ-irradiated Nanopure Diamond UV water (Pyrogens: < 0001 EU/ml, total organic carbon: < 3.0 ppb) containing 2% mouse serum (Jensen and Kembouche, 2014). The amount of particles was 2.56 mg/mL, corresponding to at a dose of 128 μg/mouse after instillation of a 50 μL volume. The suspension was then continuously sonicated on ice-bath for 16 min by use of a Branson Sonifier S-450D (Branson Ultrasonics Corp., Danbury, CT) equipped with a 13 nm disruptor horn (Model number: 101-147-037, Branson Ultrasonics Corp., Danbury, CT, USA). To obtain the two lowest doses the highest dose was diluted 3- and 9 fold, respectively, and these lower doses were re-sonicated 2 min each. To assure particle homogeneity, the suspension was administered to the animals within one hour.

2.3. Material characterisation

The hydrodynamic size distributions of the different nanomaterial suspensions were determined via Dynamic Light Scattering (DLS) on a Malvern Zetasizer Nano ZS (Malvern Instruments, UK). The data were analysed in the Dispersion Technology Software v5.0 (Malvern Instruments, UK). Size distributions were measured at 25 °C directly on the instillation suspensions. For the calculation of hydrodynamic size, the following values were used: Dispersion refractive index: 1.33; Materials refractive index: 2.9; Viscosity 1.12 cP; Material absorption: 0.1. Crystalline phases were determined by the X-ray powder diffraction XRD method on a Bruker D8 Advanced diffractometer in reflection mode with Bragg-Brentano geometry. The analysis were made using

Table 1
Physical chemical characterisation of nanomaterials.

Nanomaterials	αFe_2O_3 particle	αFe_2O_3 rod	$NiZnFe_4O_8$	$ZnFe_2O_4$	$NiFe_2O_4$	Carbon black (CB)
NRCWE-Code	NRCWE-018	NRCWE-019	NRCWE-020	NRCWE-021	NRCWE-022	Printex-90
Source	NanoAmor	NanoAmor	NanoAmor	NanoAmor	NanoAmor	Degussa-Hüls
Stock #	2520TR	8004NJ	4115FY	5710FY	4110FY	n/a
Size data [nm]	20-60[a]	40 − 130 × 250-600[a]	10-30[a]	15-30[a]	20-30[a]	14
DLS size (Z-average) [nm]	97	215	197	98	180	n/a
XRD phase	hematite	hematite	isometric magnetite	isometric magnetite	isometric magnetite	n/a
XRD-size [nm]	80	72	12	10	16	14 nm (Jacobsen et al., 2008a, 2008b; Saber et al., 2005)
Relative density; δ [g/cm^3]	5.24[a]	5.3[b]	~5.2[a]	~5.1[a]	5.368[a]	n/a
BET SSA [m^2/g]	27.7	27.4	104	87.7	86.9	229-338 (Jacobsen et al., 2008b; Saber et al., 2005)
BET-size = 6000/(BET x δ) [nm]	40.9	41.3	11.1	13.4	12.9	n/a
TGA < 110 °C [wt%]	1.97[c]	2.19[c]	3.03[c]	n/a	3.04[c]	n/a
Water loss [wt%] Oven method	1.02[c]	2.28[c]	2.74[c]	n/a	2.61[c]	n/a
LOI > 110 °C [wt%] Oven method	3.1[c]	3.12[c]	3.28[c]	n/a	3.21[c]	n/a
Total mass-loss [wt%]	4.12	5.4	6.02	5.5[d]	5.82[c]	n/a
Chemical purity [wt%]	98[a]	> 99[a]	98.5[a]	98.5[a]	98.5[a]	n/a

n/a designates: not available. [a]) Information from vendor; [b]) Assumed value from webmineral.com [c])(Clausen et al., 2019); [d]) Unpublished TGA-data data (10 °C/min; room temperature to 1000 °C, not corrected for boyancy) generated by R. Birkedal at the National Research Centre for the Working Environment as part of the EU FP7 NANODEVICE project.

$Cu_{K\alpha 1}$ X-rays (1.5406 Å) generated using a sealed Cu X-ray tube run at 40 kV and 40 mA. The analyses were made in the stepping mode stepping 0.02 ° 2°per second and data were collected using a linear PSD detector (Lynx-eye) with opening angle 3.3°. Crystallite sizes were calculated by Rietveld refinement from the data using the Topas 4.1 software (Bruker, Bremen, Germany). The specific surface areas were determined by the Brünauer Emmett and Teller (BET) analysis a commercial service from Quantachrome (Germany) using a Quantachrome Quadrasorb, resp. Quantachrome Autosorb-3 apparatus using nitrogen at 77 K as multipoint BET after degassing at 300 °C.

2.4. Animal procedures and differential counting

All animal procedures complied with the EC Directive 86/609/EEC and Danish law regulating experiments with animals (The Danish Ministry of Justice, Animal Experiments Inspectorate permission 2006/561–1123). Female C57BL/6 J BomTac mice, 7 weeks of age, and with a bw of 19 ± 1.5 g were obtained from Taconic Europe (Ejby, Denmark). Upon arrival the animals were randomised to cages containing either control animals or cages containing nanomaterial administered animals (n = 6 per cage and n = 6 per treatment group). Caging conditions were as previously described (Jacobsen et al., 2015). Briefly, the animals had ad libitum access to food (Altromin no. 1324, Christian Petersen, Denmark) and tap water. Housing was provided using polypropylene cages with Enviro-Dri bedding (Brogaarden, Gentofte, Denmark) and cage enrichment was MS wood blocks (Brogaarden, Gentofte, Denmark) and hides (Mouse House, Scanbur, Karlslunde, Denmark). The room temperature was 20 ± 2 °C and the humidity was 50 ± 20%. The animals were kept under a 12 h light: 12 h dark cycle (on from 6 a.m. to 6 p.m.). The mice were allowed one week of acclimatisation, before being administered nanomaterials by single intratracheal instillation as previously described (Jackson et al., 2011). In brief, the mice were anaesthetised by 4% isoflurane inhalation while placed on a heating plate. A volume of 50 µL particle suspension (or vehicle control, 2% mouse serum in nanopure water) was instilled followed by 150 µL air using an SGE glass syringe (250F-LT-GT, MicroLab, Aarhus, Denmark). Subsequently, breathing was monitored in order to assure that airways were not blocked. The doses were 14 µg/mouse (0.7 mg/kg bw), 43 µg/mouse (2.1 mg/kg bw) and 128 µg/mouse (6.4 mg/kg bw), except for CB for which the dose was 162 µg/mouse (8.1 mg/kg bw). After an exposure period of 1, 3 or 28 days the mice were euthanised using subcutaneous injection of Zoletil-Fentanyl. Then the thorax was opened and macroscopic abnormalities such as discolorations, ascites or bleeding were monitored. BAL was recovered by flushing the lungs twice each using 1 mL saline /25 g bw as described in (Kyjovska et al., 2015a, 2015b; Wallin et al., 2017). The BAL fluid was kept on ice until separation of fluid and cells by centrifugation at 400 x g at 4 °C for 10 min. Cells were re-suspended in 100 µL HAM-F12 medium (Prod no. 21765037, Invitrogen, Carlsbad, CA, USA) with 10% foetal bovine serum (Prod no. 10106169, Invitrogen, Carlsbad, CA, USA). For comet assay, 40 µl of this resuspension was added 160 µL of 90% HAMF12, 10% FBS, 1% Dimethyl sulfoxide and stored at −80 °C until analyses. For immune cell differential counting, 40 µL of the fresh resuspension was collected on microscope slides by centrifugation, 55 xg, 4 min using a Cytofuge 2 (StatSpin, Bie and Berntsen, Rødovre, Denmark). Cells on the slides were fixed for 5 min in 96% ethanol and stained with May-Grünwald-Giemsa stain. Slides were randomized and blinded before differentiation and counting of 200 cells per slide. The number of neutrophils as well as the number of other cell types was recorded. The total number of cells in the resuspension was measured with a NucleoCounter NC-200 (Chemometec, Allerød, Denmark) Live/Dead Assay. Due to a technical error in the Cytofuge 2, the differential cell counts failed for a number of animals as there were insufficient cell numbers on the slides. This resulted in the exclusion of a number of BAL cell composition determinations per exposures group. Lung and liver were recovered and snap frozen in liquid nitrogen and stored frozen until comet assay.

2.5. Analysis of DNA strand break levels by comet assay

Levels of DNA strand breaks were assessed in BAL cells and lung and liver tissue as tail percent DNA, measured by comet assay using the IMSTAR Pathfinder system as previously described (Jackson et al., 2013). Negative and positive controls included on all slides were A549 cells, exposed to 0 and 60 µM H_2O_2 respectively. These were included to monitor day-to-day variation and efficacy of each individual electrophoresis.

2.6. Thermodynamic chemical reaction modelling to assess the potential dissolution and redox activity of the of the Fe_2O_3 and the MFe_2O_4 spinel nanomaterials in the airways

This modelling was done using the Geochemist Workbench® v.11 (Bethke and Yeakel, 2018). Calculations were made considering a low-Ca Gambles solution (Guldberg et al., 2003) as a model for the lung lining fluid. The NM concentrations used in the calculations were derived considering the installed particle concentration and the liquid volumes in the lung lining. In the lung, a total surfactant layer volume of 13.4 µL was assumed considering a lung area of 670 cm^3 and a 0.2 µm thick surfactant layer. However, due to the 50 µL instillation volume, a total of 13.4 + 50 = 63.4 µL assumed a in the lung for the first 24 h after which, normal volume of 13.4 µL was assumed. Consequently, the average instilled particle concentrations in the lung lining fluids during instillation were on day 1: 0.2, 0.7 and 2.0 µg/µL and on day 2 to 28: 1.1, 3.2 and 9.6 µg/µL ignoring any uptake of nanomaterials by macrophages. Calculations were made of the contribution of electrons (pE = -Log([e]) to the lung-lining fluids and released elemental concentration in the lung lining fluid as function of dose. Mineral saturation limits (Q/K) given as quantity (Q) over solubility product (K) were calculated as function of dose to assess test material stabilities and the potential for phase transformations. The thermodynamic data for the calculations were taken from the Geochemist Workbench® v.11 databases, except for $NiZnFe_4O_8$, that did not exist in the database. Therefore, calculations for $NiZnFe_4O_8$ were made considering a 1:1 ratio of $NiFe_2O_4$:$ZnFe_2O_4$ and should be considered indicative. In the calculations, pH and temperature was fixed to 7.4 and 37 °C, respectively and the oxygen fugacity was set to 0.13. As a start for all calculations, the test substances and Fe was set free to vary and Cl^- to charge balance. Finally, the initial element concentrations of test materials were set to 1e-9 mmol/kg Gambles solution to allow calculations.

2.7. Statistical analysis

Physicochemical analyses were represented as ordinary arithmetic averages and standard deviations as calculated following default equations in MicroSoft Excel. Statistics in the animal study were calculated using the Graph Pad Prism 7.02 software package (Graph Pad Software Inc., La Jolla, CA, USA). Data were first tested for normality using the Shapiro-Wilk test. The *t*-test and the ANOVA test are robust against deviations from normality, therefore these were performed unless the *p* value of the Shapiro Wilks test was very low ($p < 0.001$); or unless the standard deviation was deemed very different. This was done using the F test (for two sample comparisons) or Brown-Forsythe test for three or more treatment groups ($p < 0.001$). The latter tests were calculated because the *t*-test and the ANOVA are somewhat sensitive to differences in standard deviation. In case of these described deviations in normality or in standard deviations, non-parametric Mann Whitney test (two groups) or Kruskall-Wallis (more than two groups) was applied. The data were tested so that each particle type was tested independently against the vehicle control. In order to assess differences in-between groups in one-way ANOVA or Kruskall-Wallis test, multiple comparisons post tests were applied. These were Holm-Sidak's multiple

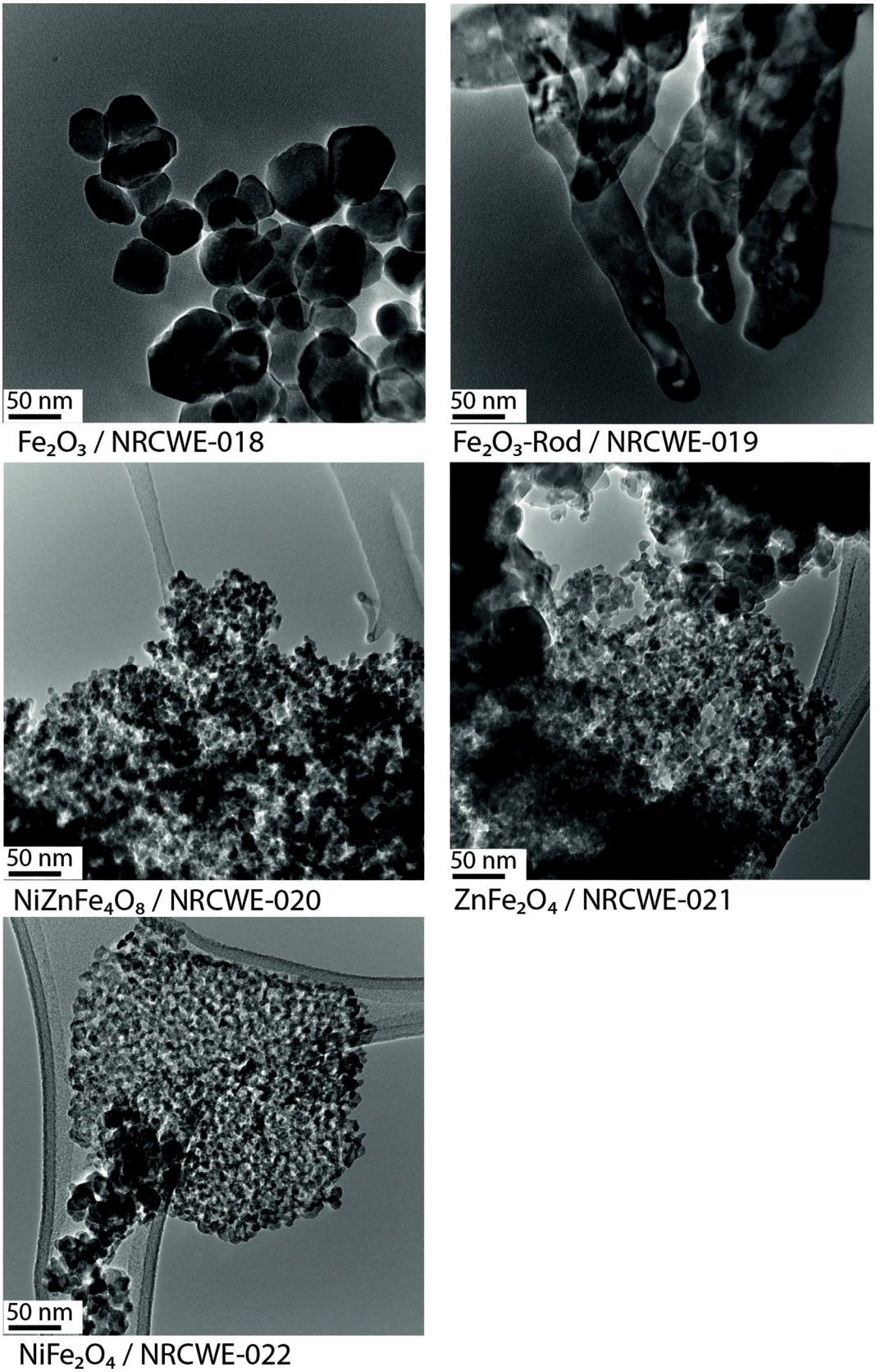

Fig. 1. TEM images of the investigated nanomaterials.

comparisons test (ANOVA) or Dunn's multiple comparisons test (Kruskall-Wallis test).

3. Results

3.1. Physical chemical characterisation

The two hematite and ferrite spinel materials were all confirmed by X-ray diffraction analysis and average crystallite sizes calculated by Rietveld refinement were in general agreement with the information provided by the vendor (Table 1). Only the Fe_2O_3 particle had larger XRD-size (80 nm) than the reported physical size. However, theoretical spherical diameters – calculated from the specific surface areas and the materials' relative densities – were smaller and within reported size ranges (Table 1). Regarding solubility, the levels of dissolved elements in bio-durability assays were not significant for Fe in Fe_2O_3 particles and Fe_2O_3 rods and for Fe, Ni and Zn in $NiZnFe_4O_8$ (data not shown). Transmission electron microscopy (TEM) analysis confirmed the rod-like morphology of the Fe_2O_3 rods and the approximately spherical shape of the other nanomaterials (Fig. 1).

3.2. Neutrophil numbers in BAL

Total cell counts in BAL as well as cell distribution by cell type are presented in Supplementary Materials (Table S1). At day 1 post-exposure, Fe_2O_3 rods and $NiZnFe_4O_8$ at highest dose, and $ZnFe_2O_4$ and $NiFe_2O_4$ at the two highest doses showed increased neutrophil numbers (Fig. 2). With increasing recovery time the absolute number of neutrophils decreased, but statistically significant levels remained at 3 days for the highest dose levels of $ZnFe_2O_4$ and $NiFe_2O_4$ (Fig. 2). At day 28 post-exposure, neutrophil influx into BAL fluid was elevated for Fe_2O_3 particles, $NiZnFe_4O_8$ and $NiFe_2O_4$ particles at highest dose (Fig. 2). At all three time points, the positive control (162 µg CB) increased neutrophil numbers in BAL as previously reported (Bengtson et al., 2017; Hadrup et al., 2017; Kyjovska et al., 2015a; Poulsen et al., 2016; Saber et al., 2012a)(Fig. 2).

We wanted to compare these data with previously compiled BAL neutrophil data from rats and mice instilled with nanoparticles (Schmid and Stoeger, 2016). For this, we converted our neutrophil data from day 1 and 28 into 1) normalised neutrophil numbers and 2) normalised lung-deposited-surface-area dose. According to the protocol described by Schmid and Stoeger: the neutrophil numbers were divided by total BAL cell counts, and the administered mass-dose was multiplied by the mass-specific BET surface area of each material (Table 1), and subsequently normalised to lung weight (cm^2/g lung; approximately 0.18 mg for C57BL/6 J mice (Schmid and Stoeger, 2016)). The study from Schmid and Stoeger includes so-called *low-solubility, low-toxicity* (LSLT) nanomaterials, which are inert nanomaterials; i.e. without specific toxicity exerted by their elemental composition. These comprise: TiO_2; amorphous SiO_2; and various types of soot particles - including *Printex 90* and *NIST SRM1650 Diesel Soot* (Schmid and Stoeger, 2016). Since the study by Schmid and Stoeger (2016) is limited to certain day-1-data, we here included new LSLT neutrophil data at day 1 and 28 previously, published by us. These data were from: a) Two types of TiO_2 (rutile, 10 nm in primary diameter, 99 m^2/g, supplier: NanoAmor, NRCWE-001; and NRCWE-001 modified to have negative surface charge; 84 m^2/g; NRCWE-002) (Wallin et al., 2017)); b) Diesel soot (108 m^2/g; NIST SRM1650) (Kyjovska et al., 2015a); and c) Carbon black CB (Printex 90) (Bourdon et al., 2012; Husain et al., 2013; Saber et al., 2012a).

Fig. 3A depicts the neutrophil cells, in percent of total BAL cells, as function of the total deposited surface area of the included Fe- and LSLT-nanomaterials at day 1. Almost all Fe-nanomaterials exhibited a dose-response effect similar to that of the LSLT nanomaterials, except for the Fe_2O_3 rods, which induced more inflammation than expected from the deposited surface area and $NiZnFe_4O_8$, which induced less inflammation than expected from the deposited surface area. At day 28,

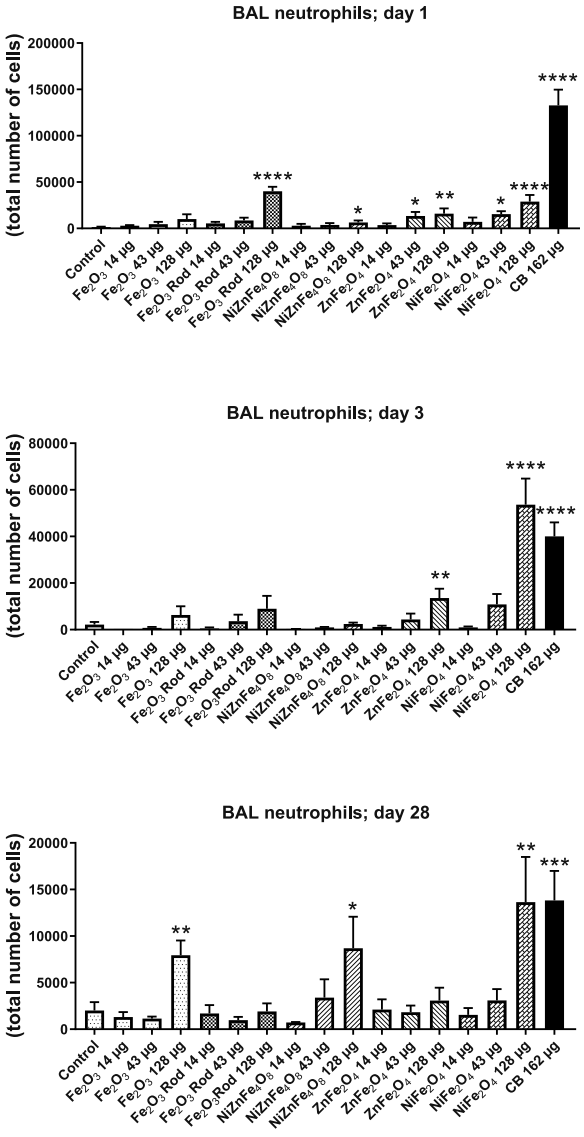

Fig. 2. Neutrophil numbers in BAL at 1, 3 and 28 days of nanomaterial exposure. Fe_2O_3 particle, Fe_2O_3 rod, $NiZnFe_4O_8$, $ZnFe_2O_4$ or $NiFe_2O_4$ were administered intratracheally to mice at 14, 43 or 128 µg/mouse. CB was administered at 162 µg/mouse. One, three or twenty-eight days later BAL fluid was collected and analysed for number of neutrophils by differential counting. Data are mean and bars represent SD. ****, ***, ** and * designates p values of < 0.0001, < 0.001, < 0.01 and < 0.05 respectively of one way ANOVA with Holm-Sidak's multiple comparisons test in case of data approaching normality and not having a highly different variation (details given in the methods section), otherwise by Kruskall-Wallis test with Dunn's multiple comparisons test. In the case of CB ****, and *** designates p values of < 0.0001, and < 0.001 respectively of t-test in case of data approaching normality and not having a highly different variation (details given in the methods section), otherwise by Mann Whitney test.

three of the five nanomaterials, Fe_2O_3, $NiFe_2O_4$ and $NiZnFe_4O_8$ nanoparticles, showed statistically significantly elevated neutrophil influx (relative to sham control) at the highest doses (Fig. 2); and the Fe_2O_3 nanoparticles were clearly above the 95% confidence level of the neutrophil levels of LSLT nanomaterials (Fig. 3B) (26% neutrophils at 200 m^2/g). This indicates that at day 28, only the Fe_2O_3 nanoparticles were more inflammogenic than expected for LSLT nanoparticles.

3.3. DNA damage

Increased DNA strand break levels were observed for Fe_2O_3 rods in

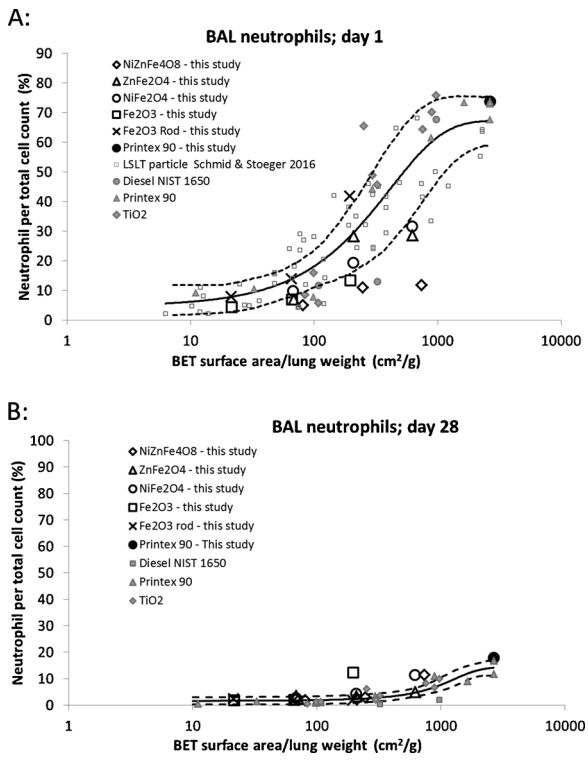

Fig. 3. Nanomaterial induced effects on neutrophil numbers in BAL depending on surface area dose. The Fe_2O_3 rod and Fe_2O_3, $NiZnFe_4O_8$, $ZnFe_2O_4$ and $NiFe_2O_4$ nanoparticle data from 1d and 28d from Fig. 2 were normalised neutrophil influx (number of neutrophils per total cell count) and surface-area-dose as described in the text. Data from the current study are presented as large open symbols (black). A) For comparison, the 1-day data were depicted with previously published neutrophil data for instilled nanoparticles with low solubility and low toxicity (LSLT) from (Schmid and Stoeger, 2016) and from our previous studies (TiO_2, Diesel NIST SRM1650 and Printex 90 from our previous studies; (Bourdon et al., 2012; Husain et al., 2013; Kyjovska et al., 2015a; Saber et al., 2012a)) It is evident, that based on the 1-day neutrophil response all of the Fe materials tested here belong to the LSLT class. **B)** At 28 days post-exposure Fe_2O_3 particles induced inflammation levels exceeding those of LSLT materials. The solid and dashed lines represent the mean and ± 95% confidence levels of the logistic curve fit of the LSLT data, respectively.

BAL cells at day 3 for the two highest doses; and for the Fe_2O_3 particle at highest dose (Fig. 4). No increases in DNA strand break levels were observed for lung or liver tissue; and the benchmark reference material, CB, did not affect levels of DNA strand breaks in any of the tissues (Figs. 4, S1, and S2). Control samples resulted in the following values for tail percent DNA (mean value ± SD)(not shown in the figure): 6.4 ± 1.9 (lung), 6.8 ± 2.1 (liver), 9.0 ± 3.7 (BAL) for the negative controls and 41.2 ± 7.9 (lung), 32.3 ± 7.9 (liver) and 26.5 ± 8.6 (BAL) for the positive controls.

3.4. Modelled solubility, transformation and redox potential of the test materials

Geochemist Workbench calculations using Gambles solution suggested that αFe_2O_3 (hematite) was insoluble and did not change the redox potential of the lung-lining fluid at any of the initial doses. $NiFe_2O_4$, $ZnFe_2O_4$, and $ZnNiFe_4O_8$ were predicted to be partially unstable resulting in partial dissolution, phase transformation/re-precipitation and redox reactivity (Supplementary Table S2). According to these calculations, $ZnFe_2O_4$, and $ZnNiFe_4O_8$ were the most reactive materials (Supplementary Table S2). An increased reactivity over time was predicted, caused by low-level dissolution of $NiFe_2O_4$ and $ZnFe_2O_4$ in both $ZnFe_2O_4$ and $NiZnFe_4O_8$ and re-precipitation as hematite

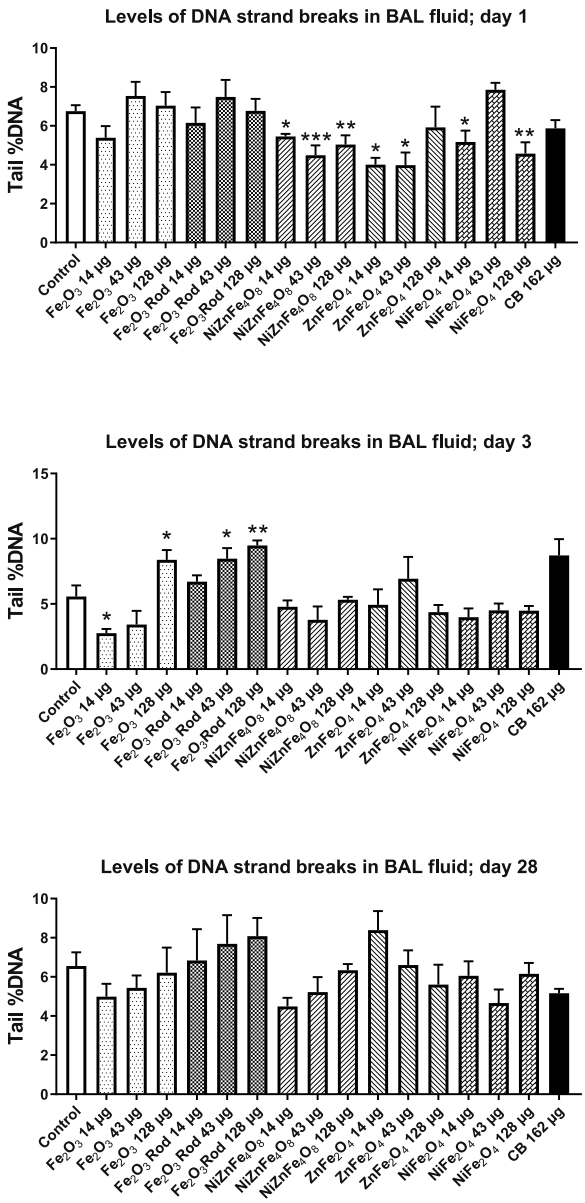

Fig. 4. Levels of DNA strand breaks in BAL fluid cells at 1, 3 and 28 days of nanomaterial exposure.
Fe_2O_3 particle, Fe_2O_3 Rod, $NiZnFe_4O_8$, $ZnFe_2O_4$ or $NiFe_2O_4$ were administered intratracheally to mice at 14, 43 or 128 µg/mouse. CB was administered at 162 µg/mouse. One, three or twenty-eight days later BAL fluid cells were prepared and levels of DNA strand breaks measured as percent DNA in the tail by comet assay. Data are mean and bars represent SD. ***, ** and * designates p values of < 0.001, < 0.01 and < 0.05 respectively of one way ANOVA with Holm-Sidak's multiple comparisons test in case of data approaching normality and not having a highly different variation (details given in the methods section), otherwise by Kruskall-Wallis test with Dunn's multiple comparisons test. In the case of CB, data were tested with t-test in case of data approaching normality and not having a highly different variation, otherwise by Mann Whitney test.

(Fe_2O_3) and/or smithsonite $ZnCO_3$. The predicted low-level dissolution of $NiFe_2O_4$ and relatively higher dissolution of $ZnFe_2O_4$ would result in low-level release of Ni and Fe ions and a higher level of Zn ion release in the lung lining fluid (Supplementary Table S2).

4. Discussion

The aim of the current investigation was to assess the toxicity of

αFe_2O_3 particles and rods; and $ZnFe_2O_4$, $NiFe_2O_4$, and $NiZnFe_4O_8$ particles, following a single intratracheal administration with follow-up periods of 1, 3, and 28 days; measured endpoints were pulmonary inflammation and DNA strand breaks. Inflammation was assessed in terms of neutrophil cell numbers in BAL and genotoxicity was assessed as DNA strand break levels in the comet assay. We have previously demonstrated that neutrophil influx is a sensitive marker of pulmonary inflammation that correlates closely with expression of genes involved in inflammatory pathways (Bourdon et al., 2012a; Hadrup et al., 2019a, 2019b; Halappanavar et al., 2019, 2011; Husain et al., 2015, 2013), as well as with acute phase response gene expression (Saber et al., 2014, 2013). Similarly, increased DNA strand break levels in the comet assay is a sensitive biomarker of DNA damage. We have previously found that carbon black and diesel exhaust particles, which induce high levels of DNA strand breaks in the comet assay, also increased the mutation frequency in a murine lung epithelial cell line (Jacobsen et al., 2011, 2008a, 2007).

4.1. Pulmonary inflammation

All of the investigated Fe-based particles were inflammogenic in a dose- and time- dependent manner, with only $NiFe_2O_4$ being inflammogenic at all the assessed time points (Fig. 2). At day 1, the Fe_2O_3 rod induced more inflammation than the Fe_2O_3 particle, even though the two particles have the same specific surface area. However, at the later time points, there was no apparent shape-related inflammation, as is expected for high-aspect ratio nanomaterials. At day 3 and 28, $NiFe_2O_4$ induced neutrophil levels that were similar to that of the positive control (162 μg CB Printex 90); albeit its surface-area-dose is approximately three fold lower than that of CB (see Fig. 3). Recently, (Schmid and Stoeger, 2016) have presented a meta-analysis of studies on pulmonary neutrophil influx at day 1 after intratracheal instillation including some twenty different nanomaterials. It was found that surface area – not mass, volume or number - is by far the most relevant dose metric of acute pulmonary inflammation. This confirms the results of previous studies on bio-persistent nano- and micro-sized particles (Oberdorster et al., 2005; Stoeger et al., 2009, 2007). Moreover, Schmid and Stoeger identified a class of *low-solubility, low-toxicity* (LSLT) nanomaterials; a class often referred to as "*inert materials without specific toxicity*". This LSLT class included: a) six types of soot (including Printex 90 and Diesel soot NIST SRM1650), b) three types of TiO_2 (including P25), c) amorphous silica, and d) polystyrene nanoparticles. As seen on Fig. 3A, the surface-area-dose-dependent neutrophil influx of the Fe_2O_3, $ZnFe_2O_4$, and $NiFe_2O_4$ nanomaterials determined at day 1 in this study were within (or just outside) the ± 95% confidence range of LSLT particle-induced neutrophil influx as determined by Schmid and Stoeger, whereas $NiZnFe_4O_8$ induced less inflammation than expected from the specific surface area. This suggests that all these materials can be classified in the same category as other biologically low reactive (inert) low-solubility materials. On day 28, the Fe_2O_3 nanoparticles (not rods) induced higher inflammogenicity than predicted from the specific surface area of LSLT particles (Fig. 3B). However, low-level solubility, leading to some release of Ni, Fe and Zn ions was predicted by solubility modelling of the $NiFe_2O_4$, $ZnFe_2O_4$ and $NiZnFe_4O_8$ particles in the low-Ca Gambles surrogate lung-lining fluids, whereas the Fe_2O_3 nanoparticles were predicted to be stable and insoluble (Table S2). Thus, the inflammation observed for Fe_2O_3 particles at day 28 and not for Fe_2O_3 rods appears not to be due to toxicity of low levels of dissolved Fe, because then the same response should be expected from both Fe_2O_3 nanomaterials. However, this observation relies on a single data point (the highest dose at day 28). For Fe_2O_3 rods and $NiFe_2O_4$, and $ZnFe_2O_4$ particles, the observed neutrophil influx was similar to the levels observed for LSLT particles. Although $NiZnFe_4O_8$ induced somewhat less inflammation than predicted by the deposited surface area, $NiZnFe_4O_8$ could be grouped with the LSLT particles for practical reasons. Moreover, since the applied surface area dose for Fe_2O_3 rods (diameter: 40 − 150 nm; length: 250 − 600 nm) and Fe_2O_3 particles (20 − 60 nm) is almost identical – and since only the Fe_2O_3 particles showed statistically significantly increased inflammation, the increased and potential shape-specific toxicity observed for the relatively short and thick Fe_2O_3 nanorods at day 1 were not observed after 28 days. This is in general agreement with results for carbon nanotubes, where enhanced and persistent inflammation is mostly reported for thick and presumable rigid long fibres (> 5 μm) (Knudsen et al., 2018; Poland et al., 2008; Poulsen et al., 2016, 2015). Studies have shown that different sizes and shapes of Fe_2O_3 result in activation of different toxicological mechanisms (Cai et al., 2018). Fe_2O_3 is also not fully stable in biological tissue resulting in partial dissolution (Lartigue et al., 2013) and biotransformation from e.g., super-parametric maghemite into poorly-magnetic iron species occur (Levy et al., 2011). Potentially, even the crystalline polymorph of Fe_2O_3 (αFe_2O_3; hematite or γFe_2O_3; maghemite) may play a role on its behaviour (Auffan et al., 2009).

Most of the literature on Fe-related particle toxicity has used mass as the dose metric. In the next part, we compare our observations with mass-based findings, even though surface area is likely the better dose metric for prediction of inflammation. Rats inhaled 15 − 20 nm of Fe_3O_4 for 4 h and an increase in BAL neutrophils was measured at the only tested dose 640 mg/m^3 (Srinivas et al., 2012). With a much lower mass concentration, 0.09 mg/m^3 for 18 h, 72 nm Fe-based particles (likely Fe_2O_3) did not affect BAL neutrophil numbers in rats (Zhou et al., 2003). With a larger Fe_3O_4 particle, 300 − 600 nm, in a 13-week inhalation study, neutrophils in BAL increased at 100 mg/m^3, but not at 50 mg/m^3 (Pauluhn, 2009). Fe_3O_4 with a mass median aerodynamic diameter of 1.3 μm was investigated in a 13-week rat inhalation study. The mass concentrations were 5, 17 or 52 mg/m^3. Neutrophils and protein in BAL increased at the highest dose (Pauluhn, 2012). Rats inhaled Fe_3O_4 with a median mass diameter of 1.4 μm and with mass concentrations of 32 or 100 mg/m^3. BAL neutrophil numbers increased at the highest dose (Pauluhn and Wiemann, 2011). Rats were exposed to Fe_2O_3 (~30 nm) as dry powder sprayed directly into both nasal passages twice daily for 3 days. The daily dose was 8.5 mg/kg bw; A range of serum biochemical endpoints were affected; and severe damage was observed in liver and lung tissues of Fe_2O_3 treated rats (Lijuan et al., 2010). Concerning the intratracheal instillation model for exposure, rats were given Fe_2O_3 particles of either 22 or 280 nm at 0.8 or 20 mg/kg bw. Neutrophil numbers in BAL was increased across the doses and sizes at both 1 and 7 days post exposure (Zhu et al., 2008). Mice were intratracheally instilled with 0.2, 0.6 or 2 mg/kg bw of 20 nm Fe_2O_3, no effect was seen on neutrophil numbers in BAL fluid 24 h later (Pirela et al., 2013). Iron oxide nanoparticles containing both (Fe(II) and Fe (III)) (presumably magnetite; Fe_3O_4) were given to rats by intratracheal instillation at 1 or 5 mg/kg bw. Body weight gain was decreased at both dose levels. The only pathological finding was weak pulmonary fibrosis at both dose levels (Szalay et al., 2012). Using intratracheal instillation, Sayes et al. found increased neutrophil numbers in BAL in rat at 5 mg/kg bw using carbonyl Fe (metallic Fe) of 561 nm (BET surface area: 2.5 m^2/g) at day 1 (Sayes et al., 2007). Rice et al. found increased neutrophil numbers in BAL at 16 and 48 h at 0.06 mg Fe/kg bw, when rats were dosed with ferrous sulphate (likely $FeSO_4$ dissolved into Fe) (Rice et al., 2001). $FeSO_4$ did not induce neutrophil influx at 0.06 mg Fe/kg bw in rats at 4, 24, 48 or 96 h after instillation (Wallenborn et al., 2008), or at even higher doses of 4.8 μg Fe/mouse (0.16 mg Fe/kg bw) at 1, 3, 7 or 14 days after instillation (Prieditis and Adamson, 2002). Thus, altogether, pulmonary exposure to Fe – as Fe_2O_3 or in other metallic, oxide or water-soluble forms – seems to induce low levels of inflammation. Our no-observed-adverse-effect level of 43 μg (~2 mg/kg bw) of the Fe_2O_3 materials is in line with those observed previously (Pirela et al., 2013; Zhu et al., 2008). In addition, our data shows that inflammation caused by pulmonary dosing of Fe_2O_3 particles and short and relatively thick nanorods can be predicted by the deposited surface area of LSLT materials; consistent with the low predicted solubility of Fe_2O_3 and the low inflammogenic potential of Fe

ions. The fact that we only see moderately elevated effects at 28 days relative to LSLT materials, and only at the highest applied dose, suggests that Fe_2O_3 is not very inflammogenic.

To the best of our knowledge, literature on pulmonary toxicity is currently not available for $ZnFe_2O_4$, $NiFe_2O_4$ and $NiZnFe_4O_8$ nanomaterials. Nonetheless, there are data on other particles containing either Ni or Zn. Inhalation of Ni (dosed as $NiCl_2$) at 0.6 mg/m^3 for 4 months, 5 days/week, 6 h/day in, rabbits, increased neutrophil numbers in BAL (Johansson et al., 1992). In addition, intratracheal instillation of insoluble NiO nanoparticles in rats has been demonstrated to increase neutrophils in BAL at 0.7 mg/kg bw at 24 h and 4 weeks after instillation (Cho et al., 2012); and a similar effect was observed with 0.5 mg/kg bw (24 h after) and 0.16 mg/kg bw (28 days) (Cho et al., 2010). Increased neutrophils were also observed in rats at 24 h after instillation of 0.7 mg/kg bw NiO nanoparticles and of 0.6 mg/kg bw $NiCl_2$ (Lee et al., 2016). Thus, pulmonary exposure to both dissolved Ni ions and to insoluble NiO nanoparticles cause inflammation. ZnO is likely dissolved in vivo in lungs leading to release of Zn^{2+} as discussed in (Ho et al., 2011) and shown in dissolution studies (Koltermann-Jülly et al., 2018). Inhaled ZnO particles in different sizes cause neutrophil influx in BAL in rat and mouse at 1–12 mg/m^3 (Adamcakova-Dodd et al., 2015; Chen et al., 2015; Chuang et al., 2014; Conner et al., 1988; Ho et al., 2011; Larsen et al., 2016). Pulmonary inflammation was also found in a range of intratracheal studies with ZnO particles of different sizes and surface coatings. Lowest-observed-adverse-effect levels were 0.3–1 mg/kg bw in rat and mouse at 24 h of exposure (Cho et al., 2012; Niels Hadrup et al., 2019a, 2019b; Jacobsen et al., 2015; Warheit et al., 2009) Regarding later time points, 1 week to 3 months, no or low levels of inflammation have been observed with ZnO particles (Cho et al., 2011, 2010; Niels Hadrup et al., 2019a, 2019b; Warheit et al., 2009). Thus, pulmonary exposure to ZnO and the subsequent release of Zn^{2+} causes short-term inflammation.

Solubility is an important predictor of toxicity and experimentally derived dissolution rates can usually be used to predict the pulmonary biodurability and clearance (Koltermann-Jülly et al., 2018; Utembe et al., 2015).The literature data suggest that exposure to both Ni- and Zn-oxide and their dissolved ions induce pulmonary inflammation. However, our modelling data suggested negligible solubility in the lung lining fluid, and the observed inflammation induced by $NiFe_2O_4$, $ZnFe_2O_4$ and $NiZnFe_4O_8$ particles was consistent with the level of inflammation predicted by the deposited surface area as predicted for LSLT particles both 1 and 28 days post-exposure. Therefore, there is no indication of solubility-related acute and short-term toxicity for these particles.

4.2. Levels of DNA strand breaks

Increased levels of DNA strand breaks were only observed in BAL fluid cells, not in lung or liver tissue. Increased levels of DNA strand breaks were only observed on day 3, where the two types of Fe_2O_3 induced DNA strand breaks. Previously, magnetite particles with a mass-specific BET surface area of 7 m^2/g have been reported to induce tumours in rats at high dose (167 mg/kg bw) during 131 weeks of observation (Pott et al., 1994). Magnetite (Fe_3O_4) contains both Fe^{2+} and Fe^{3+} whereas Fe_2O_3 contains only Fe^{3+}. Nevertheless, our data, taken together with the Pott study, warrant more pulmonary genotoxicity data on Fe_2O_3. Inhalation of dissolved Ni ions has induced adrenal gland and adrenal medulla tumours and bronchial gland hyperplasia when dosed to mice or rats in the range of 0.4–1.25 mg/m^3 in studies ranging from 140 h to 3000 h (Dunnick et al., 1995; Horie et al., 1985; NTP, 1996; Oller et al., 2008). Using intratracheal instillation, Pott et al. reported formation of lung tumours in rats with NiO (likely insoluble), nickel subsulfide (these likely act as ions) as well as nickel powder (size not reported). The lowest-observed-adverse-effect levels were: NiO: 167 mg Ni/kg bw, nickel subsulfide: 3 mg Ni/kg bw, and nickel powder: 20 mg Ni/kg bw (Pott et al., 1987). NiO particles of 1000 nm at 100 mg/kg bw were found to induce lung tumours at 131 weeks of exposure in rats (Pott et al., 1994). Notably, these doses are much higher than those used in the current study, and thus an absence of DNA damage of the Ni-containing phases in the current work are in line with the literature.

ZnO particles of 13 and 36 nm did not induce increased levels of DNA strand breaks at mass concentrations of 58 or 53 mg/m^3 in mice after 1 h of inhalation; with estimated airway depositions of 78 μg and 17 μg, for the 13 and 36 nm particles, respectively (Larsen et al., 2016). In addition, 8-Oxo-2′-dG formation caused by ZnO, 35 and 250 nm, was investigated in rat after 6 h of inhalation. Increases were found at 12 (35 nm) and 45 mg/m^3 (250 nm), respectively (with no effects at 3.7 (35 nm) and 11.5 mg/m^3 (250 nm) (Ho et al., 2011). Regarding intratracheal instillation, ZnO of 50 nm increased 8-Oxo-2′-dG levels at 33 mg/kg bw in rats (Chuang et al., 2014); a dose 3 fold higher than our highest dose (9 mg/kg bw). Taking our own and literature data into account, we conclude that more data are needed before it can be firmly determined whether Zn has a pulmonary genotoxic and carcinogenic potential.

Altogether, our data suggests that Fe_2O_3has a genotoxic potential, but we observed no additional contribution to genotoxicity from the short and relatively thick nanorod. Since DNA damage was observed for both the Fe_2O_3 particle and for the corresponding rod, the rod shape did not seem to contribute to the observed genotoxicity.

5. Conclusion

We assessed the pulmonary toxicity Fe_2O_3, $ZnFe_2O_4$, $NiFe_2O_4$ and $NiZnFe_4O_8$ nanomaterials in mice. One day post-exposure, all the studied nanomaterials were inflammogenic at or near levels predicted by the deposited surface area of low solubility low toxicity (LSLT) particles. Both Fe_2O_3 nanomaterials induced genotoxicity in BAL cells at 3 days post-exposure. To our knowledge, besides magnetite (Fe_3O_4), this is the first study of the pulmonary toxicity of M-Fe_2O_4 spinel nanomaterials.

Transparency document

The Transparency document associated with this article can be found in the online version.

CRediT authorship contribution statement

Niels Hadrup: Formal analysis, Writing - original draft, Writing - review & editing. **Anne T. Saber:** Investigation, Writing - review & editing. **Zdenka O. Kyjovska:** Formal analysis, Investigation, Writing - review & editing. **Nicklas R. Jacobsen:** Investigation, Writing - review & editing. **Minnamari Vippola:** Formal analysis, Investigation, Writing - review & editing. **Essi Sarlin:** Formal analysis, Investigation, Writing - review & editing. **Yaobo Ding:** Formal analysis, Investigation, Writing - review & editing. **Otmar Schmid:** Conceptualization, Formal analysis, Writing - original draft, Writing - review & editing. **Håkan Wallin:** Conceptualization, Writing - review & editing, Supervision, Funding acquisition. **Keld A. Jensen:** Conceptualization, Formal analysis, Writing - original draft, Writing - review & editing, Supervision, Project administration. **Ulla Vogel:** Conceptualization, Formal analysis, Writing - original draft, Writing - review & editing, Supervision, Project administration, Funding acquisition.

Acknowledgements

Technical assistance from Michael Guldbrandsen, Eva Terrida, Natacha Synnøve Olsen, Anne-Karin Asp and Elzbieta Christiansen, Signe H. Nielsen and Yahia Kembouche, was greatly appreciated. Renie Birkedal (formerly employed at NRCWE) is gratefully acknowledged for conducting X-ray diffraction analysis of the test materials and initial

thermogravimetric analysis. This work has been financed by the EU FP7 NANODEVICE project (Grant agreement no. CP-IP 211464-2), Danish Centre for Nanosafety 1 (Danish Working Environment Research Fund, grant# 20110092173-3), Danish Centre for Nanosafety 2 and the EU Horizon 2020 project SmartNanoTox, grant agreement No. 686098.

Appendix A. Supplementary data

Supplementary material related to this article can be found, in the online version, at doi:https://doi.org/10.1016/j.etap.2019.103303.

References

Adamcakova-Dodd, A., Monick, M.M., Powers, L.S., Gibson-Corley, K.N., Thorne, P.S., 2015. Effects of prenatal inhalation exposure to copper nanoparticles on murine dams and offspring. Part Fibre Toxicol 12, 30. https://doi.org/10.1186/s12989-015-0105-5.

Al-Qubaisi, M.S., Rasedee, A., Flaifel, M.H., Ahmad, S.H.J., Hussein-Al-Ali, S., Hussein, M.Z., Eid, E.E.M., Zainal, Z., Saeed, M., Ilowefah, M., Fakurazi, S., Mohd Isa, N., El Zowalaty, M.E., 2013. Cytotoxicity of nickel zinc ferrite nanoparticles on cancer cells of epithelial origin. Int. J. Nanomedicine 8, 2497–2508. https://doi.org/10.2147/IJN.S42367.

AlSalka, Y., Granone, L.I., Ramadan, W., Hakki, A., Dillert, R., Bahnemann, D.W., 2019. Iron-based photocatalytic and photoelectrocatalytic nano-structures: facts, perspectives, and expectations. Appl. Catal. B Environ. 244, 1065–1095. https://doi.org/10.1016/j.apcatb.2018.12.014.

Auffan, M., Rose, J., Wiesner, M.R., Bottero, J.-Y., 2009. Chemical stability of metallic nanoparticles: a parameter controlling their potential cellular toxicity in vitro. Environ. Pollut. 157, 1127–1133. https://doi.org/10.1016/j.envpol.2008.10.002.

Aziz, M.H., Fatima, M., Ali, S.M., Atif, M., Noreen, Z., Ahmad, I., Shaheen, F., Ali, A., Baig, M.R., Ullah, H., Abbas, G., Alkhuraiji, T.S., 2018. In vitro cytotoxicity of magnetic spinel nanoferrites (CoMgFe 2 O 4) against HepG2 cells. J. Nanoelectron. Optoelectron. 13, 251–257. https://doi.org/10.1166/jno.2018.2227.

Bárcena, C., Sra, A.K., Chaubey, G.S., Khemtong, C., Liu, J.P., Gao, J., 2008. Zinc ferrite nanoparticles as MRI contrast agents. Chem. Commun 2224. https://doi.org/10.1039/b801041b.

Bengtson, S., Knudsen, K.B., Kyjovska, Z.O., Berthing, T., Skaug, V., Levin, M., Koponen, I.K., Shivayogimath, A., Booth, T.J., Alonso, B., Pesquera, A., Zurutuza, A., Thomsen, B.L., Troelsen, J.T., Jacobsen, N.R., Vogel, U., 2017. Differences in inflammation and acute phase response but similar genotoxicity in mice following pulmonary exposure to graphene oxide and reduced graphene oxide. PLoS One. 12, e0178355.

Bethke, C.M., Yeakel, S., 2018. The Geochemist's Workbench® Release 11.

Bourdon, J.A., Halappanavar, S., Saber, A.T., Jacobsen, N.R., Williams, A., Wallin, H., Vogel, U., Yauk, C.L., 2012a. Hepatic and pulmonary toxicogenomic profiles in mice intratracheally instilled with carbon black nanoparticles reveal pulmonary inflammation, acute phase response, and alterations in lipid homeostasis. Toxicol.Sci. 127, 474–484.

Bourdon, J.A., Saber, A.T., Jacobsen, N.R., Jensen, K.A., Madsen, A.M., Lamson, J.S., Wallin, H., Moller, P., Loft, S., Yauk, C.L., Vogel, U.B., 2012b. Carbon black nanoparticle instillation induces sustained inflammation and genotoxicity in mouse lung and liver. Part Fibre.Toxicol. 9, 5.

Cai, X., Dong, J., Liu, J., Zheng, H., Kaweeteerawat, C., Wang, F., Ji, Z., Li, R., 2018. Multi-hierarchical profiling the structure-activity relationships of engineered nanomaterials at nano-bio interfaces. Nat. Commun. 9, 4416. https://doi.org/10.1038/s41467-018-06869-9.

Chen, J.K., Ho, C.C., Chang, H., Lin, J.F., Yang, C.S., Tsai, M.H., Tsai, H.T., Lin, P., 2015. Particulate nature of inhaled zinc oxide nanoparticles determines systemic effects and mechanisms of pulmonary inflammation in mice. Nanotoxicology. 9, 43–53.

Cho, W.S., Duffin, R., Howie, S.E., Scotton, C.J., Wallace, W.A., MacNee, W., Bradley, M., Megson, I.L., Donaldson, K., 2011. Progressive severe lung injury by zinc oxide nanoparticles; the role of Zn2+ dissolution inside lysosomes. Part Fibre.Toxicol. 8, 27.

Cho, W.S., Duffin, R., Poland, C.A., Duschl, A., Oostingh, G.J., MacNee, W., Bradley, M., Megson, I.L., Donaldson, K., 2012. Differential pro-inflammatory effects of metal oxide nanoparticles and their soluble ions in vitro and in vivo; zinc and copper nanoparticles, but not their ions, recruit eosinophils to the lungs. Nanotoxicology. 6, 22–35.

Cho, W.S., Duffin, R., Poland, C.A., Howie, S.E., MacNee, W., Bradley, M., Megson, I.L., Donaldson, K., 2010. Metal oxide nanoparticles induce unique inflammatory footprints in the lung: important implications for nanoparticle testing. Environ.Health Perspect. 118, 1699–1706.

Chuang, H.C., Juan, H.T., Chang, C.N., Yan, Y.H., Yuan, T.H., Wang, J.S., Chen, H.C., Hwang, Y.H., Lee, C.H., Cheng, T.J., 2014. Cardiopulmonary toxicity of pulmonary exposure to occupationally relevant zinc oxide nanoparticles. Nanotoxicology. 8, 593–604.

Clausen, P.A., Kofoed-Sørensen, V., Nørgaard, A.W., Sahlgren, N.M., Jensen, K.A., 2019. Thermogravimetry and mass spectrometry of extractable organics from manufactured nanomaterials for identification of potential coating components. Materials (Basel). 12, 3657. https://doi.org/10.3390/ma12223657.

Conner, M.W., Flood, W.H., Rogers, A.E., Amdur, M.O., 1988. Lung injury in guinea pigs caused by multiple exposures to ultrafine zinc oxide: changes in pulmonary lavage fluid. J.Toxicol.Environ.Health 25, 57–69.

Ding, Y., Kuhlbusch, T.A.J., Van Tongeren, M., Jiménez, A.S., Tuinman, I., Chen, R., Alvarez, I.L., Mikolajczyk, U., Nickel, C., Meyer, J., Kaminski, H., Wohlleben, W., Stahlmecke, B., Clavaguera, S., Riediker, M., 2017. Airborne engineered nanomaterials in the workplace—a review of release and worker exposure during nanomaterial production and handling processes. J. Hazard. Mater. 322, 17–28. https://doi.org/10.1016/j.jhazmat.2016.04.075.

Dunnick, J.K., Elwell, M.R., Radovsky, A.E., Benson, J.M., Hahn, F.F., Nikula, K.J., Barr, E.B., Hobbs, C.H., 1995. Comparative carcinogenic effects of nickel subsulfide, nickel oxide, or nickel sulfate hexahydrate chronic exposures in the lung. Cancer Res. 55, 5251–5256.

ECHA, 2019. European Union Observatory for Nanomaterial: Catalogue of Cosmetic Ingredients [WWW Document]. URL. https://euon.echa.europa.eu/catalogue-of-cosmetic-ingredients.

Gopal Reddy, C.V., Manorama, S.V., Rao, V.J., 2000. Preparation and characterization of ferrites as gas sensor materials. J. Mater. Sci. Lett. 19, 775–778.

Guldberg, M., Madsen, A.L., Sebastian, K., Fellman, J., Potter, R., Bauer, J., Searl, A., Maquin, B., Jubb, G., 2003. EURIMA test guideline: In-vitro acellular dissolution of man-made vitreous silicate fibres. Glas. Sci. Technol. -Frankfurt am Main 76, 199–205.

Hadrup, N., Bengtson, S., Jacobsen, N.R., Jackson, P., Nocun, M., Saber, A.T., Jensen, K.A., Wallin, H., Vogel, U., 2017. Influence of dispersion medium on nanomaterial-induced pulmonary inflammation and DNA strand breaks: investigation of carbon black, carbon nanotubes and three titanium dioxide nanoparticles. Mutagenesis 32. https://doi.org/10.1093/mutage/gex042.

Hadrup, N., Rahmani, F., Jacobsen, N., Saber, A., Jackson, P., Bengtson, S.A.W., Wallin, H., Halappanavar, S., Vogel, U., 2019a. Acute Phase Response and Inflammation Following Pulmonary Exposure to Low Doses of Zinc Oxide Nanoparticles in Mice. Nanotoxicology Accepted F. https://doi.org/10.1080/17435390.2019.1654004.

Hadrup, Niels, Rahmani, F., Jacobsen, N.R., Saber, A.T., Jackson, P., Bengtson, S., Williams, A., Wallin, H., Halappanavar, S., Vogel, U., 2019b. Acute phase response and inflammation following pulmonary exposure to low doses of zinc oxide nanoparticles in mice. Nanotoxicology 13, 1275–1292. https://doi.org/10.1080/17435390.2019.1654004.

Halappanavar, S., Jackson, P., Williams, A., Jensen, K.A., Hougaard, K.S., Vogel, U., Yauk, C.L., Wallin, H., 2011. Pulmonary response to surface-coated nanotitanium dioxide particles includes induction of acute phase response genes, inflammatory cascades, and changes in microRNAs: a toxicogenomic study. Environ.Mol.Mutagen. 52, 425–439.

Halappanavar, S., Rahman, L., Nikota, J., Poulsen, S.S., Ding, Y., Jackson, P., Wallin, H., Schmid, O., Vogel, U., Williams, A., 2019. Ranking of nanomaterial potency to induce pathway perturbations associated with lung responses. NanoImpact 14, 100158. https://doi.org/10.1016/j.impact.2019.100158.

Halappanavar, S., Saber, A.T., Decan, N., Jensen, K.A., Wu, D., Jacobsen, N.R., Guo, C., Rogowski, J., Koponen, I.K., Levin, M., Madsen, A.M., Atluri, R., Snitka, V., Birkedal, R.K., Rickerby, D., Williams, A., Wallin, H., Yauk, C.L., Vogel, U., 2015. Transcriptional profiling identifies physicochemical properties of nanomaterials that are determinants of the in vivo pulmonary response. Environ. Mol. Mutagen. 56, 245–264.

Ham, S., Kim, S., Lee, N., Kim, P., Eom, I., Tsai, P.-J., Lee, K., Yoon, C., 2015. Comparison of nanoparticle exposure levels based on facility type—small-Scale laboratories, large-scale manufacturing workplaces, and unintended nanoparticle-emitting workplaces. Aerosol Air Qual. Res. 15, 1967–1978. https://doi.org/10.4209/aaqr.2015.03.0141.

Ho, M., Wu, K.Y., Chein, H.M., Chen, L.C., Cheng, T.J., 2011. Pulmonary toxicity of inhaled nanoscale and fine zinc oxide particles: mass and surface area as an exposure metric. Inhal.Toxicol. 23, 947–956.

Horie, A., Haratake, J., Tanaka, I., Kodama, Y., Tsuchiya, K., 1985. Electron microscopical findings with special reference to cancer in rats caused by inhalation of nickel oxide. Biol.Trace Elem.Res. 7, 223–239.

Hosni, N., Zehani, K., Brazuna, R.P., Moscovici, J., Bessais, L., Maghraoui-Meherzi, H., 2018. Synthesis of (2D) MNPs nanosheets of nickel ferrite using a low-cost co-precipitation process. Mater. Sci. Eng. B 232–235, 48–54. https://doi.org/10.1016/j.mseb.2018.10.012.

Husain, M., Kyjovska, Z.O., Bourdon-Lacombe, J., Saber, A.T., Jensen, K.A., Jacobsen, N.R., Williams, A., Wallin, H., Halappanavar, S., Vogel, U., Yauk, C.L., 2015. Carbon black nanoparticles induce biphasic gene expression changes associated with inflammatory responses in the lungs of C57BL/6 mice following a single intratracheal instillation. Toxicol. Appl. Pharmacol. 289, 573–588.

Husain, M., Saber, A.T., Guo, C., Jacobsen, N.R., Jensen, K.A., Yauk, C.L., Williams, A., Vogel, U., Wallin, H., Halappanavar, S., 2013. Pulmonary instillation of low doses of titanium dioxide nanoparticles in mice leads to particle retention and gene expression changes in the absence of inflammation. Toxicol. Appl. Pharmacol. 269, 250–262.

IARC, 2012. IARC Monographs Volume 100C NICKEL AND NICKEL COMPOUNDS.

Ito, A., Shinkai, M., Honda, H., Kobayashi, T., 2005. Medical application of functionalized magnetic nanoparticles. J. Biosci. Bioeng. 100, 1–11. https://doi.org/10.1263/jbb.100.1.

Jackson, P., Lund, S.P., Kristiansen, G., Andersen, O., Vogel, U., Wallin, H., Hougaard, K.S., 2011. An experimental protocol for maternal pulmonary exposure in developmental toxicology. Basic Clin. Pharmacol.Toxicol. 108, 202–207.

Jackson, P., Pedersen, L.M., Kyjovska, Z.O., Jacobsen, N.R., Saber, A.T., Hougaard, K.S., Vogel, U., Wallin, H., 2013. Validation of freezing tissues and cells for analysis of DNA strand break levels by comet assay. Mutagenesis 28, 699–707. https://doi.org/10.1093/mutage/get049.

Jacobsen, N.R., Moller, P., Cohn, C.A., Loft, S., Vogel, U., Wallin, H., 2008a. Diesel exhaust particles are mutagenic in FE1-MutaMouse lung epithelial cells. Mutat. Res. 641, 54–57.

Jacobsen, N.R., Pojana, G., White, P., Moller, P., Cohn, C.A., Korsholm, K.S., Vogel, U.,

Marcomini, A., Loft, S., Wallin, H., 2008b. Genotoxicity, cytotoxicity, and reactive oxygen species induced by single-walled carbon nanotubes and C(60) fullerenes in the FE1-Mutatrade markMouse lung epithelial cells. Environ. Mol. Mutagen. 49, 476–487.
Jacobsen, N.R., Saber, A.T., White, P., Moller, P., Pojana, G., Vogel, U., Loft, S., Gingerich, J., Soper, L., Douglas, G.R., Wallin, H., 2007. Increased mutant frequency by carbon black, but not quartz, in the lacZ and cII transgenes of muta mouse lung epithelial cells. Environ. Mol. Mutagen. 48, 451–461.
Jacobsen, N.R., Stoeger, T., van den, B.S., Saber, A.T., Beyerle, A., Vietti, G., Mortensen, A., Szarek, J., Budtz, H.C., Kermanizadeh, A., Banerjee, A., Ercal, N., Vogel, U., Wallin, H., Moller, P., 2015. Acute and subacute pulmonary toxicity and mortality in mice after intratracheal instillation of ZnO nanoparticles in three laboratories. Food Chem.Toxicol. 85, 84–95.
Jacobsen, N.R., White, P.A., Gingerich, J., Moller, P., Saber, A.T., Douglas, G.R., Vogel, U., Wallin, H., 2011. Mutation spectrum in FE1-MUTA(TM) Mouse lung epithelial cells exposed to nanoparticulate carbon black. Environ. Mol. Mutagen. 52, 331–337.
Jensen, K.A., Kembouche, Y., 2014. The ENPRA Dispersion Protocol for NANoREG.
Johansson, A., Curstedt, T., Jarstrand, C., Camner, P., 1992. Alveolar macrophages and lung lesions after combined exposure to nickel, cobalt, and trivalent chromium. Environ. Health Perspect. 97, 215–219.
Knudsen, K.B., Berthing, T., Jackson, P., Poulsen, S.S., Mortensen, A., Jacobsen, N.R., Skaug, V., Szarek, J., Hougaard, K.S., Wolff, H., Wallin, H., Vogel, U., 2018. Physicochemical predictors of Multi-Walled Carbon Nanotube-induced pulmonary histopathology and toxicity one year after pulmonary deposition of 11 different Multi-Walled Carbon Nanotubes in mice. Basic Clin. Pharmacol. Toxicol. 124 (2), 211–227. https://doi.org/10.1111/bcpt.13119.
Koltermann-Jülly, J., Keller, J.G., Vennemann, A., Werle, K., Müller, P., Ma-Hock, L., Landsiedel, R., Wiemann, M., Wohlleben, W., 2018. Abiotic dissolution rates of 24 (nano)forms of 6 substances compared to macrophage-assisted dissolution and in vivo pulmonary clearance: grouping by biodissolution and transformation. NanoImpact 12, 29–41. https://doi.org/10.1016/j.impact.2018.08.005.
Koponen, I.K., Koivisto, A.J., Jensen, K.A., 2015. Worker exposure and high time-resolution analyses of process-related submicrometre particle concentrations at mixing stations in two paint factories. Ann. Occup. Hyg. 59, 749–763. https://doi.org/10.1093/annhyg/mev014.
Kubo, O., Ido, T., Yokoyama, H., 1982. Properties of Ba ferrite particles for perpendicular magnetic recording media. IEEE Trans. Magn. 18, 1122–1124. https://doi.org/10.1109/TMAG.1982.1062007.
Kyjovska, Z.O., Jacobsen, N.R., Saber, A.T., Bengtson, S., Jackson, P., Wallin, H., Vogel, U., 2015a. DNA strand breaks, acute phase response and inflammation following pulmonary exposure by instillation to the diesel exhaust particle NIST1650b in mice. Mutagenesis 30, 499–507.
Kyjovska, Z.O., Jacobsen, N.R., Saber, A.T., Bengtson, S., Jackson, P., Wallin, H., Vogel, U., 2015b. DNA damage following pulmonary exposure by instillation to low doses of carbon black (Printex 90) nanoparticles in mice. Environ. Mol. Mutagen. 56, 41–49.
Larsen, S.T., Jackson, P., Poulsen, S.S., Levin, M., Jensen, K.A., Wallin, H., Nielsen, G.D., Koponen, I.K., 2016. Airway irritation, inflammation, and toxicity in mice following inhalation of metal oxide nanoparticles. Nanotoxicology 10, 1254–1262.
Lartigue, L., Alloyeau, D., Kolosnjaj-Tabi, J., Javed, Y., Guardia, P., Riedinger, A., Péchoux, C., Pellegrino, T., Wilhelm, C., Gazeau, F., 2013. Biodegradation of Iron oxide nanocubes: high-resolution in situ monitoring. ACS Nano 7, 3939–3952. https://doi.org/10.1021/nn305719y.
Latorre, M., Rinaldi, C., 2009. Applications of magnetic nanoparticles in medicine: magnetic fluid hyperthermia. P. R. Health Sci. J. 28, 227–238.
Lee, S., Hwang, S.-H., Jeong, Jiyoung, Han, Y., Kim, S.-H., Lee, D.-K., Lee, H.-S., Chung, S.-T., Jeong, Jayoung, Roh, C., Huh, Y.S., Cho, W.-S., 2016. Nickel oxide nanoparticles can recruit eosinophils in the lungs of rats by the direct release of intracellular eotaxin. Part. Fibre Toxicol. 13, 30. https://doi.org/10.1186/s12989-016-0142-8.
Levy, M., Luciani, N., Alloyeau, D., Elgrabli, D., Deveaux, V., Pechoux, C., Chat, S., Wang, G., Vats, N., Gendron, F., Factor, C., Lotersztajn, S., Luciani, A., Wilhelm, C., Gazeau, F., 2011. Long term in vivo biotransformation of iron oxide nanoparticles. Biomaterials 32, 3988–3999. https://doi.org/10.1016/j.biomaterials.2011.02.031.
Martin, J., Bello, D., Bunker, K., Shafer, M., Christiani, D., Woskie, S., Demokritou, P., 2015. Occupational exposure to nanoparticles at commercial photocopy centers. J. Hazard. Mater. 298, 351–360. https://doi.org/10.1016/j.jhazmat.2015.06.021.
Moller, P., Jensen, D.M., Christophersen, D.V., Kermanizadeh, A., Jacobsen, N.R., Hemmingsen, J.G., Danielsen, P.H., Karottki, D.G., Roursgaard, M., Cao, Y., Jantzen, K., Klingberg, H., Hersoug, L.G., Loft, S., 2015. Measurement of oxidative damage to DNA in nanomaterial exposed cells and animals. Environ. Mol. Mutagen. 56, 97–110.
NTP, 1996. NTP toxicology and carcinogenesis studies of nickel oxide (CAS No. 1313-99-1) in F344 rats and B6C3F1 mice (Inhalation studies). Natl. Toxicol. Program.Tech. Rep. Ser 451, 1–381.
Oberdorster, G., Oberdorster, E., Oberdorster, J., 2005. Nanotoxicology: an emerging discipline evolving from studies of ultrafine particles. Environ. Health Perspect. 113, 823–839.
Oller, A.R., Kirkpatrick, D.T., Radovsky, A., Bates, H.K., 2008. Inhalation carcinogenicity study with nickel metal powder in Wistar rats. Toxicol. Appl. Pharmacol. 233, 262–275.
Pauluhn, J., 2012. Subchronic inhalation toxicity of iron oxide (magnetite, Fe(3) O(4)) in rats: pulmonary toxicity is determined by the particle kinetics typical of poorly soluble particles. J. Appl. Toxicol. 32, 488–504.
Pauluhn, J., 2009. Retrospective analysis of 4-week inhalation studies in rats with focus on fate and pulmonary toxicity of two nanosized aluminum oxyhydroxides (boehmite) and pigment-grade iron oxide (magnetite): the key metric of dose is particle mass and not particle sur. Toxicology 259, 140–148.
Pauluhn, J., Wiemann, M., 2011. Siderite (FeCO(3)) and magnetite (Fe(3)O(4)) overload-dependent pulmonary toxicity is determined by the poorly soluble particle not the iron content. Inhal. Toxicol. 23, 763–783.
Phumying, S., Labuayai, S., Swatsitang, E., Amornkitbamrung, V., Maensiri, S., 2013. Nanocrystalline spinel ferrite (MFe2O4, M = Ni, Co, Mn, Mg, Zn) powders prepared by a simple aloe vera plant-extracted solution hydrothermal route. Mater. Res. Bull. 48, 2060–2065. https://doi.org/10.1016/j.materresbull.2013.02.042.
Pirela, S., Molina, R., Watson, C., Cohen, J.M., Bello, D., Demokritou, P., Brain, J., 2013. Effects of copy center particles on the lungs: a toxicological characterization using a Balb/c mouse model. Inhal. Toxicol. 25, 498–508. https://doi.org/10.3109/08958378.2013.806614.
Poland, C.A., Duffin, R., Kinloch, I., Maynard, A., Wallace, W.A.H., Seaton, A., Stone, V., Brown, S., Macnee, W., Donaldson, K., 2008. Carbon nanotubes introduced into the abdominal cavity of mice show asbestos-like pathogenicity in a pilot study. Nat. Nanotechnol. 3, 423–428. https://doi.org/10.1038/nnano.2008.111.
Pott, F., Dungworth, D.L., Heinrich, U., Muhle, H., Kamino, K., Germann, P.G., Roller, M., Rippe, M., Mohr, U., 1994. Lung tumours in rats after intratracheal instillation of dusts. Ann. Occup. Hyg. 38, 357–363.
Pott, F., Ziem, U., Reiffer, F.J., Huth, F., Ernst, H., Mohr, U., 1987. Carcinogenicity studies in fibers, metal-compounds, and some other dusts in rats. Exp. Pathol. 32, 129–152.
Poulsen, S.S., Jackson, P., Kling, K., Knudsen, K.B., Skaug, V., Kyjovska, Z.O., Thomsen, B.L., Clausen, P.A., Atluri, R., Berthing, T., Bengtson, S., Wolff, H., Jensen, K.A., Wallin, H., Vogel, U., 2016. Multi-walled carbon nanotube physicochemical properties predict pulmonary inflammation and genotoxicity. Nanotoxicology. 10, 1263–1275.
Poulsen, S.S., Knudsen, K.B., Jackson, P., Weydahl, I.E.K., Saber, A.T., Wallin, H., Vogel, U., 2017. Multi-walled carbon nanotube-physicochemical properties predict the systemic acute phase response following pulmonary exposure in mice. PLoS One 12, e0174167. https://doi.org/10.1371/journal.pone.0174167.
Poulsen, S.S., Saber, A.T., Williams, A., Andersen, O., Kobler, C., Atluri, R., Pozzebon, M.E., Mucelli, S.P., Simion, M., Rickerby, D., Mortensen, A., Jackson, P., Kyjovska, Z.O., Molhave, K., Jacobsen, N.R., Jensen, K.A., Yauk, C.L., Wallin, H., Halappanavar, S., Vogel, U., 2015. MWCNTs of different physicochemical properties cause similar inflammatory responses, but differences in transcriptional and histological markers of fibrosis in mouse lungs. Toxicol. Appl. Pharmacol. 284, 16–32.
Prasad, G.K., Kumar, J.P., Pandey, L.K., Singh, B., 2017. Nanoporous materials for the remediation of industrial toxic chemicals. Adv. Porous Mater. 5, 1–16. https://doi.org/10.1166/apm.2017.1132.
Prieditis, H., Adamson, I.Y.R., 2002. Comparative pulmonary toxicity of various soluble metals found in urban particulate dusts. Exp. Lung Res. 28, 563–576. https://doi.org/10.1080/01902140290096782.
Rice, T.M., Clarke, R.W., Godleski, J.J., Al-Mutairi, E., Jiang, N.F., Hauser, R., Paulauskis, J.D., 2001. Differential ability of transition metals to induce pulmonary inflammation. Toxicol. Appl. Pharmacol. 177, 46–53. https://doi.org/10.1006/taap.2001.9287.
Saber, A.T., Bornholdt, J., Dybdahl, M., Sharma, A.K., Loft, S., Vogel, U., Wallin, H., 2005. Tumor necrosis factor is not required for particle-induced genotoxicity and pulmonary inflammation. Arch.Toxicol. 79, 177–182.
Saber, A.T., Jacobsen, N.R., Jackson, P., Poulsen, S.S., Kyjovska, Z.O., Halappanavar, S., Yauk, C.L., Wallin, H., Vogel, U., 2014. Particle-induced pulmonary acute phase response may be the causal link between particle inhalation and cardiovascular disease. Wiley. Interdiscip. Rev. Nanomed. Nanobiotechnol 6, 517–531.
Saber, A.T., Jacobsen, N.R., Mortensen, A., Szarek, J., Jackson, P., Madsen, A.M., Jensen, K.A., Koponen, I.K., Brunborg, G., Gutzkow, K.B., Vogel, U., Wallin, H., 2012a. Nanotitanium dioxide toxicity in mouse lung is reduced in sanding dust from paint. Part Fibre.Toxicol. 9, 4.
Saber, A.T., Jensen, K.A., Jacobsen, N.R., Birkedal, R., Mikkelsen, L., Moller, P., Loft, S., Wallin, H., Vogel, U., 2012b. Inflammatory and genotoxic effects of nanoparticles designed for inclusion in paints and lacquers. Nanotoxicology. 6, 453–471.
Saber, A.T., Koponen, I.K., Jensen, K.A., Jacobsen, N.R., Mikkelsen, L., Moller, P., Loft, S., Vogel, U., Wallin, H., 2012c. Inflammatory and genotoxic effects of sanding dust generated from nanoparticle-containing paints and lacquers. Nanotoxicology. 6, 776–788.
Saber, A.T., Lamson, J.S., Jacobsen, N.R., Ravn-Haren, G., Hougaard, K.S., Nyendi, A.N., Wahlberg, P., Madsen, A.M., Jackson, P., Wallin, H., Vogel, U., 2013. Particle-induced pulmonary acute phase response correlates with neutrophil influx linking inhaled particles and cardiovascular risk. PLoS One 8, e69020.
Saber, A.T., Mortensen, A., Szarek, J., Koponen, I.K., Levin, M., Jacobsen, N.R., Pozzebon, M.E., Mucelli, S.P., Rickerby, D.G., Kling, K., Atluri, R., Madsen, A.M., Jackson, P., Kyjovska, Z.O., Vogel, U., Jensen, K.A., Wallin, H., 2016. Epoxy composite dusts with and without carbon nanotubes cause similar pulmonary responses, but differences in liver histology in mice following pulmonary deposition. Part Fibre.Toxicol. 13, 37.
Sayes, C.M., Reed, K.L., Warheit, D.B., 2007. Assessing toxicity of fine and nanoparticles: comparing in vitro measurements to in vivo pulmonary toxicity profiles. Toxicol. Sci. 97, 163–180. https://doi.org/10.1093/toxsci/kfm018.
Schmid, O., Stoeger, T., 2016. Surface area is the biologically most effective dose metric for acute nanoparticle toxicity in the lung. J. Aerosol Sci. 99, 133–143. https://doi.org/10.1016/j.jaerosci.2015.12.006.
Srinivas, A., Rao, P.J., Selvam, G., Goparaju, A., Murthy, P.B., Reddy, P.N., 2012. Oxidative stress and inflammatory responses of rat following acute inhalation exposure to iron oxide nanoparticles. Hum. Exp. Toxicol. 31, 1113–1131.
Stoeger, T., Schmid, O., Takenaka, S., Schulz, H., 2007. Inflammatory response to TiO2 and carbonaceous particles scales best with BET surface area. Environ. Health Perspect. 115, A290 1; author reply A291-2.
Stoeger, T., Takenaka, S., Frankenberger, B., Ritter, B., Karg, E., Maier, K., Schulz, H., Schmid, O., 2009. Deducing in vivo toxicity of combustion-derived nanoparticles

from a cell-free oxidative potency assay and metabolic activation of organic compounds. Environ. Health Perspect. 117, 54–60. https://doi.org/10.1289/ehp.11370.

Szalay, B., Tátrai, E., Nyírő, G., Vezér, T., Dura, G., 2012. Potential toxic effects of iron oxide nanoparticles in in vivo and in vitro experiments. J. Appl. Toxicol. 32, 446–453. https://doi.org/10.1002/jat.1779.

Tomitaka, A., Hirukawa, A., Yamada, T., Morishita, S., Takemura, Y., 2009. Biocompatibility of various ferrite nanoparticles evaluated by in vitro cytotoxicity assays using HeLa cells. J. Magn. Magn. Mater. 321, 1482–1484. https://doi.org/10.1016/j.jmmm.2009.02.058.

Utembe, W., Potgieter, K., Stefaniak, A.B., Gulumian, M., 2015. Dissolution and biodurability: important parameters needed for risk assessment of nanomaterials. Part. Fibre Toxicol. 12, 11. https://doi.org/10.1186/s12989-015-0088-2.

Vesterdal, L.K., Folkmann, J.K., Jacobsen, N.R., Sheykhzade, M., Wallin, H., Loft, S., Moller, P., 2010. Pulmonary exposure to carbon black nanoparticles and vascular effects. Part Fibre.Toxicol. 7, 33.

Wallenborn, J.G., Evansky, P., Shannahan, J.H., Vallanat, B., Ledbetter, A.D., Schladweiler, M.C., Richards, J.H., Gottipolu, R.R., Nyska, A., Kodavanti, U.P., 2008. Subchronic inhalation of zinc sulfate induces cardiac changes in healthy rats. Toxicol. Appl. Pharmacol. 232, 69–77.

Wallin, H., Kyjovska, Z.O., Poulsen, S.S., Jacobsen, N.R., Saber, A.T., Bengtson, S., Jackson, P., Vogel, U., 2017. Surface modification does not influence the genotoxic and inflammatory effects of TiO2 nanoparticles after pulmonary exposure by instillation in mice. Mutagenesis 32, 47–57.

Lijuan, Wang, Lin, Wang, Ding, W., Zhang, F., 2010. Acute toxicity of ferric oxide and zinc oxide nanoparticles in rats. J. Nanosci. Nanotechnol. 10, 8617–8624. https://doi.org/10.1166/jnn.2010.2483.

Warheit, D.B., Sayes, C.M., Reed, K.L., 2009. Nanoscale and fine zinc oxide particles: can in vitro assays accurately forecast lung hazards following inhalation exposures? Environ.Sci.Technol. 43, 7939–7945.

Xing, M., Zhang, Y., Zou, H., Quan, C., Chang, B., Tang, S., Zhang, M., 2015. Exposure characteristics of ferric oxide nanoparticles released during activities for manufacturing ferric oxide nanomaterials. Inhal. Toxicol. 27, 138–148. https://doi.org/10.3109/08958378.2014.1001535.

Zhou, Y.M., Zhong, C.Y., Kennedy, I.M., Pinkerton, K.E., 2003. Pulmonary responses of acute exposure to ultrafine iron particles in healthy adult rats. Environ.Toxicol. 18, 227–235.

Zhu, M.-T., Feng, W.-Y., Wang, B., Wang, T.-C., Gu, Y.-Q., Wang, M., Wang, Y., Ouyang, H., Zhao, Y.-L., Chai, Z.-F., 2008. Comparative study of pulmonary responses to nano- and submicron-sized ferric oxide in rats. Toxicology 247, 102–111. https://doi.org/10.1016/j.tox.2008.02.011.